



ARTICLE

Thermoelastic Structural Topology Optimization Based on Moving Morphable Components Framework

Jun Yan^{1,3}, Qi Xu¹, Zhirui Fan¹, Zunyi Duan^{2,*}, Hongze Du¹ and Dongling Geng¹

¹Department of Engineering Mechanics, State Key Laboratory of Structural Analysis for Industrial Equipment, International Research Center for Computational Mechanics, Dalian University of Technology, Dalian, 116024, China

²Institute of Structural Health Monitoring and Control, School of Mechanics, Civil Engineering & Architecture, Northwestern Polytechnical University, Xi'an, 710072, China

³Ningbo Research Institute of Dalian University of Technology, Ningbo, 315016, China

*Corresponding Author: Zunyi Duan. Email: duanzzy@nwpu.edu.cn

Received: 13 April 2021 Accepted: 21 May 2021

ABSTRACT

This study investigates structural topology optimization of thermoelastic structures considering two kinds of objectives of minimum structural compliance and elastic strain energy with a specified available volume constraint. To explicitly express the configuration evolution in the structural topology optimization under combination of mechanical and thermal load conditions, the moving morphable components (MMC) framework is adopted. Based on the characteristics of the MMC framework, the number of design variables can be reduced substantially. Corresponding optimization formulation in the MMC topology optimization framework and numerical solution procedures are developed for several numerical examples. Different optimization results are obtained with structural compliance and elastic strain energy as objectives, respectively, for thermoelastic problems. The effectiveness of the proposed optimization formulation is validated by the numerical examples. It is revealed that for the optimization design of the thermoelastic structural strength, the objective function with the minimum structural strain energy can achieve a better performance than that from structural compliance design.

KEYWORDS

Thermoelastic structure; topology optimization; moving morphable components; minimum structural compliance; minimum strain energy

1 Introduction

Structural topology optimization is effective to create novel structural configurations. It has been extensively utilized in various industrial applications, such as aerospace, shipbuilding, automobile industries, precision equipment, and micro-electro-mechanical systems [1–4]. In the aerospace industry particularly, structural topology optimization has been widely applied to reduce the weight of aircrafts to achieve better economic benefits. However, with the harsh service environments in supersonic speed, the friction between the wall outside an aircraft and the



atmosphere will result in relatively high temperature [5]. The high temperature in a structure will produce significant thermal stresses and may cause structural failure, which cannot be ignored in the design processes. Therefore, to reduce the weight and thermal stress of thermoelastic structures simultaneously, the topology optimization design of thermoelastic structures are studied extensively.

Rodrigues et al. [6] pioneered the studies of thermoelastic optimization; they investigated the topology optimization of a two-dimensional linear elastic structure under thermal loads by the asymptotic homogenization approach. A corresponding study showed that the optimized topologies depended significantly on the temperature differential even for simple models. Sigmund et al. [7] investigated the distribution of three-phase materials under the action of thermal loads using the homogenization method and proved that structures with extremely high thermal expansion properties can be obtained by partly sacrificing the material stiffness. Li et al. [8,9] developed an evolutionary structural optimization method to perform thermoelastic optimization. Cho et al. [10] investigated a weakly coupled thermoelastic problem using the coupled field adjoint sensitivity analysis method, which reduced the computing cost significantly compared with other sensitivity analysis methods. Chung et al. [11] studied the topology optimization of structures undergoing large deformations due to thermal and mechanical loads, which demonstrated how temperature changes affected the optimized design of the large-deforming structures. Considering the effect of temperature changes, Deng et al. [12] and Yan et al. [13] utilized concurrent multiscale formulations to optimize the configurations of macroscale topologies and microscale materials. Li et al. [14] studied the multiscale optimization based on level set approach in thermomechanical environment and indicated that the porous material is consistently found to be favored for a coupled multi-physics problem. Zhu et al. [15] proposed a temperature-constrained topology optimization for thermo-mechanical coupled problems and revealed that the temperature constraints play an important role in relevant problems. For more reviews regarding thermoelastic design optimization, readers can refer to Wu et al. [16–18].

For thermoelastic structural topology optimization, minimum structural compliance, which equals to maximum stiffness design in structural optimization only with mechanical loads as an objective function has been adopted in the above mentioned studies. However, Pedersen et al. [19,20] reported that for thermoelastic structures, the same optimized design cannot yield good performances of maximum structural strength and minimum structural compliance simultaneously. It is challenging to regard the minimum compliance of the structure as the objective function because the structural compliance can neither represent the displacement of the structure nor the effective stress under a thermo-mechanical load; as such, the physical meaning of the structural compliance optimization formulation for the thermoelastic problems will be insignificant. Deaton et al. [21] also reported that using the compliance indicator as the objective function is no longer suitable. For some typically used thermoelastic structures, such as the engine hump-washed structure for embedded engine aircraft under large temperature loading. Subsequently, a stress-based design of thermal structures had been presented by Deaton et al. [22] via topology optimization, which can efficiently dispose stress constraints under the combination of thermal and mechanical loads. Zhang et al. [23] investigated two different optimization formulations with minimum structural compliance and elastic strain energy as the objective functions of topology optimization of a thermoelastic structure based on RAMP formulation, in which numerical studies showed that the objective function with minimum elastic strain energy was more suitable for reducing the Mises stress than the minimum structural compliance. Meng et al. [24] studied the stress constrained thermo-elastic topology optimization in a non-uniform temperature field by

proposed stabilizing control schemes and indicated that the compliance minimization design with stress constraints is appropriate to achieve balance between stress level and structural stiffness.

Another concern is that the thermal load is a design-dependent load, which means that the load changes considerably during the optimization iteration procedure. However, as the density-based method is used to solve the topology optimization of thermoelastic problems, the parasitic effect for low densities will occur [25]. Hence, a modified power-law model is usually required to obtain better optimization results. Density-based methods poses some other challenges, summarized as follows. Firstly, a precise geometry is difficult to obtain because of the implicitly expressed and large area of “gray” densities in the optimized structures; furthermore, it is difficult to establish a direct link between the optimization models and computer-aided-design modeling system. Secondly, the number of design variables is relatively large, especially for three-dimensional problems. Lastly, the density-based approach analysis model and optimization model are strongly coupled; this may yield some numerical difficulties, such as the checkboard pattern. Xia et al. [26] studied the thermoelastic problem to solve the problems of “gray” and checkboard pattern by the level set method and obtained a smooth geometric boundary; however, the topology optimization is still performed in an implicit framework in this approach. To solve the challenges of topology optimization methods above, Guo et al. [27] established a moving morphable components (MMC)-based topology optimization framework. Compared with the existing methods, the key aspect of the MMC-based framework is that some explicit geometric parameters can be used to describe the topology of a structure. The design domain can be composed of a set of morphable components that can move, overlap, and disappear freely. The position, inclination, layout, and shape of components can be changed within the prescribed design domain to derive the optimal topology. Zhang et al. [28] utilized the ersatz material model and presented a new topology optimization approach based on the MMC framework; furthermore, they presented a 188 line Matlab code for implementing this approach. Based on the isogeometric analysis (IGA) technique, Zhang et al. [29] and Zhang et al. [30] developed a new explicit topology optimization framework of moving morphable void (MMV), and then studied the topology optimization problem of 3D shell structure under stress constraints. Takaloozadeh et al. [31] proposed a topological derivative approach based on the MMC framework and presented several topology optimization problems, such as stress-based and thermoelastic structural compliance optimizations.

In this study, the MMC-based framework is utilized for thermoelastic topology optimization problems considering the minimum structural compliance and elastic strain energy as the objective functions, respectively, under a specified available volume constraint. The remainder of the paper is organized as follows. In Section 2, the MMC-based topology optimization framework is briefly reviewed, and the topology description function is elucidated. Section 3 describes the problem formulation for different objective functions based on the MMC method. Some strategies for the numerical implementation of the present study are described in Section 4. Section 5 presents some numerical examples to illustrate the effectiveness of the proposed method and the physical meaning of the different objective functions.

2 Brief Introduction of the MMC-Based Framework

Compared with other density-based and node-based topology optimization methods, the MMC topology optimization framework [27] is based on a series of components as the basic building blocks of the design domain, and the geometric parameters of each component are recognized as the design variables. The final structural topology can be obtained simultaneously by optimizing the parameters of the components (such as the thickness, length, and inclined angle),

and changing the layout of the components in the specified design domain through moving, morphing, blending, and overlapping between multiple components. Therefore, the MMC-based framework can accommodate the shape, size, and topology optimization.

As shown in Fig. 1, the design domain comprises a series of components with explicit boundaries, where the geometric parameters are the center coordinates (x_{0i}, y_{0i}) , length L_i , inclined angle θ_i , and thickness $f(x')$. Additionally, $f(x') = t^1$ implies that the component is described by a uniform thickness. The geometric parameters above are the design variables in the MMC-based topology optimization framework.

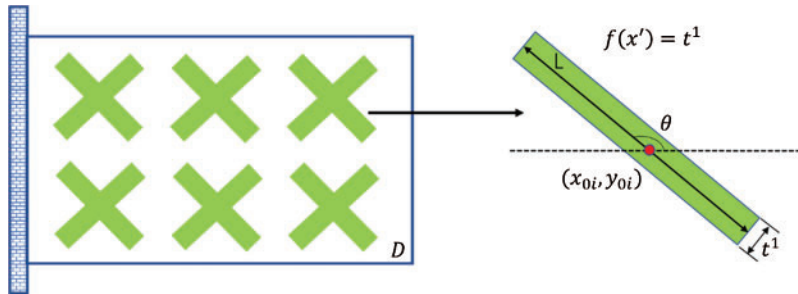


Figure 1: Basic components of MMC-based topology optimization framework [28]

In Fig. 1, as an example, each component comprises 5 design variables and 12 components exist; therefore, the total number of design variables in the design domain is $12 \times 5 = 60$. However, if using the density-based method, the number of design variables depends on the finite element mesh, usually in the order of thousands. Therefore, compared with traditional density-based topology optimization methods, the MMC-based framework reduces the number of design variables significantly, which is another advantage of the MMC-based framework.

In the MMC-based topology optimization framework, each component in the prescribed design domain is described by the topology description functions (TDF) ϕ_i as

$$\begin{cases} \phi_i(\mathbf{x}) > 0 & \text{if } \mathbf{x} \in \Omega_i \\ \phi_i(\mathbf{x}) = 0 & \text{if } \mathbf{x} \in \partial\Omega_i \\ \phi_i(\mathbf{x}) < 0 & \text{if } \mathbf{x} \in D/\Omega_i, \end{cases} \quad (1)$$

where \mathbf{x} represents the coordinates of any point in the design domain, Ω_i is the region occupied by the i -th component within the prescribed design domain D , and $\partial\Omega_i$ is the boundary of the i -th component.

For each component, the TDF can be described as

$$\phi_i(x, y) = \left(\frac{x'}{L_i}\right)^p + \left(\frac{y'}{f(x')}\right)^p - 1, \quad (2)$$

where p is a relatively large even integer number to sharpen the boundary of a component, in this study, $p = 6$. Because the components in the design domain are placed at a certain angle, a relationship between the local coordinates (x', y') of the component and the global coordinates

(x, y) of the structure must be established, as shown in Fig. 2; subsequently, the local coordinates (x', y') can be written as

$$\begin{cases} x' \\ y' \end{cases} = \begin{bmatrix} \cos\theta_i & \sin\theta_i \\ -\sin\theta_i & \cos\theta_i \end{bmatrix} \begin{cases} x - x_{0i} \\ y - y_{0i} \end{cases} \quad (3)$$

Based on the description of a single component, the structural topology description in a given design domain can be expressed as follows:

$$\begin{cases} \phi(\mathbf{x}) > 0 & \text{if } \mathbf{x} \in \Omega \\ \phi(\mathbf{x}) = 0 & \text{if } \mathbf{x} \in \partial\Omega \\ \phi(\mathbf{x}) < 0 & \text{if } \mathbf{x} \in D/\Omega, \end{cases} \quad (4)$$

where Ω denotes the occupied design domain by a set of components Ω_i ($i = 1, 2, \dots, n$) fabricated using a solid material, $\phi(\mathbf{x}) = \max(\phi_1, \dots, \phi_n)$, where n denotes the total number of components.

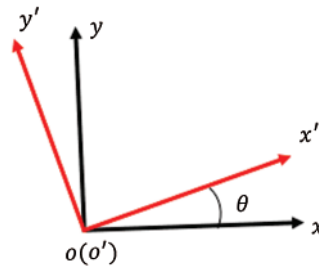


Figure 2: Relationship between local and global coordinates

3 Mathematical Formulation for two Types of Objective Functions

Under the MMC-based topology optimization framework, the general topology optimization problem can be formulated as follows [27]:

$$\begin{aligned} \text{Find: } & \mathbf{a} = ((\mathbf{a}^1)^T, \dots, (\mathbf{a}^i)^T, \dots, (\mathbf{a}^n)^T)^T \\ \text{Minimize: } & I = I(\mathbf{a}) \\ \text{Subject to: } & g_j(\mathbf{a}) \leq 0, \quad j = 1, \dots, k. \quad \mathbf{a} \in \mathcal{U}_a, \end{aligned} \quad (5)$$

where \mathbf{a} denotes the vector of the design variables, with \mathbf{a}^i ($i = 1, \dots, n$) = $(x_{0i}, y_{0i}, L_i, \theta_i, f(x'))^T$; \mathcal{U}_a represents the admissible sets of \mathbf{a} ; g_j is the j -th constraint function.

For a thermoelastic structural topology optimization, two types of objective function formulations are presented herein that accounts for the combination effects of thermal and mechanical loads based on the MMC framework. The objective functions are the minimum structural compliance and elastic strain energy, respectively. From the comparison of the optimization results of the two optimization objectives, we investigate the physical meanings of the different objective functions and determine an objective function that is more suitable for the topology optimization of thermoelastic structures. The detailed formulations of the two types of objective functions are presented as follows.

3.1 Mathematical Formulation with Minimum Structural Compliance

When minimizing structural compliance with a specified available volume constraint based on the combination of thermal and mechanical loads, the corresponding mathematical formulation can be written as follows:

$$\text{Minimize : } C = \sum_{i=1}^n \int_{\Omega^i \setminus (\cup_{1 \leq j < i} (\Omega^i \cap \Omega^j))} \mathbf{F}_{\text{th}}^i \cdot \mathbf{u} dV + \int_{\Gamma_t} \mathbf{F}_m \cdot \mathbf{u} dS$$

Subjected to:

$$\begin{aligned} & \sum_{i=1}^n \int_{\Omega^i \setminus (\cup_{1 \leq j < i} (\Omega^i \cap \Omega^j))} \boldsymbol{\sigma}(\mathbf{u}) \cdot \boldsymbol{\varepsilon}(\mathbf{v}) dV \\ & = \sum_{i=1}^n \int_{\Omega^i \setminus (\cup_{1 \leq j < i} (\Omega^i \cap \Omega^j))} \mathbf{F}_{\text{th}}^i \cdot \mathbf{v} dV + \int_{\Gamma_t} \mathbf{F}_m \cdot \mathbf{v} dS \\ & \forall \mathbf{v} \in \mathcal{U}_{\text{ad}}, V(\mathbf{a}) \leq \bar{V}, \mathbf{a} \in \mathcal{U}_a, \mathbf{u} = \bar{\mathbf{u}}, \text{ on } \Gamma_u, \end{aligned} \quad (6)$$

where \mathbf{u} and \mathbf{v} denote the displacement field and the corresponding test function defined on $\Omega = \cup_{i=1}^n \Omega^i$ with $\mathcal{U}_{\text{ad}} = \{\mathbf{v} \mid \mathbf{H}(\mathbf{a}), \mathbf{v} = 0 \text{ on } \Gamma_u\}$, respectively, \mathbf{H} is the Heaviside function. \mathbf{F}_{th}^i and \mathbf{F}_m represent the thermal load density of the i -th component and the mechanical load (surface traction on Neumann boundary Γ_t), respectively. $\boldsymbol{\varepsilon}$ and $\boldsymbol{\sigma}$ represents the stress and strain vector, respectively. The symbol \bar{V} denotes the upper limit of the material volume, and $\bar{\mathbf{u}}$ is the prescribed displacement on the Dirichlet boundary Γ_u . The structural compliance represents the total work performed by the specified load (mechanical load, thermal load, etc.).

3.2 Mathematical Formulation with Minimum Elastic Strain Energy

When minimizing elastic strain energy as the objective function with a specified available volume constraint based on the combination of thermal and mechanical loads, the corresponding mathematical formulation can be written as follows:

$$\text{Minimize : } \Phi = \sum_{i=1}^n \int_{\Omega^i \setminus (\cup_{1 \leq j < i} (\Omega^i \cap \Omega^j))} (\boldsymbol{\varepsilon} - \boldsymbol{\varepsilon}_{\text{th}})^T \mathbf{D}^i (\boldsymbol{\varepsilon} - \boldsymbol{\varepsilon}_{\text{th}}) dV$$

Subject to:

$$V(\mathbf{a}) \leq \bar{V}, \mathbf{a} \in \mathcal{U}_a \quad (7)$$

where $\boldsymbol{\varepsilon}$ is the total strain vector of the structure, and $\boldsymbol{\varepsilon}_{\text{th}}$ represents the thermal strain vector caused by the thermal load, \mathbf{D}^i represents the constitutive matrix of the i -th component.

According to [23], the strain energy in Eq. (7) can also be written as follows:

$$\Phi = \sum_{i=1}^n \int_{\Omega^i \setminus (\cup_{1 \leq j < i} (\Omega^i \cap \Omega^j))} \boldsymbol{\sigma}^T (\mathbf{D}^i)^{-1} \boldsymbol{\sigma} dV \quad (8)$$

As shown in Eq. (8), σ represents the stress vector, to some extent, the strain energy measures the stressed state of a thermoelastic structure.

4 Numerical Implementation Strategies

In this section, the finite element analysis and sensitivity analysis for topology optimization of a thermoelastic structure are presented based on the MMC topology optimization framework.

4.1 Finite Element Analysis of Objective Functions Based on an Ersatz Material Model

The MMC-based topology optimization framework is a boundary evolution-based topology optimization method, and the ersatz material model is typically applied for finite element analysis to enhance computational efficiency. The specified design domain is discretized by four-node bilinear elements; based on the method, the TDF values at four nodes of each element can be calculated as illustrated in Fig. 3.

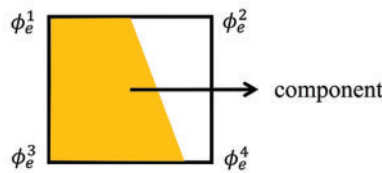


Figure 3: Component occupies the e -th element

Subsequently, the equivalent Young’s modulus of an element can be expressed as [28]

$$E^e = \frac{E \left(\sum_{\zeta=1}^4 (H(\phi_e^\zeta))^q \right)}{4} \tag{9}$$

where E is the Young’s modulus of the base material; q is an integer, where in the present study, $q = 2$. H is the Heaviside function and $\phi_e^\zeta, \zeta = 1, \dots, 4$ are the values of the TDF function of the whole structure (i.e., $\phi(x)$) at four nodes of element e . In the present study, the piecewise continuous Heaviside function is used as follows:

$$H(z) = \begin{cases} 1 & \text{if } z > \xi \\ \frac{3(1-\alpha)}{4} \cdot \left(\frac{z}{\xi} - \frac{z^3}{3\xi^3} \right) + \frac{(1+\alpha)}{2} & \text{if } -\xi \leq z \leq \xi \\ \alpha & \text{otherwise} \end{cases} \tag{10}$$

where ξ is a parameter used to control the regularization magnitude; α is a small positive non-zero value ($\alpha = 0.001$) to ensure the non-singularity of the global stiffness matrix; z is the TDF value of an arbitrary point within the design domain.

The objective function in Eq. (6) (**structural compliance**) under a combination of thermal and mechanical loads can be discretized into the finite element format as follows:

$$C = \mathbf{F}_{th}^T \mathbf{U} + \mathbf{F}_m^T \mathbf{U} \tag{11}$$

where \mathbf{U} denotes the total nodal displacement vector caused by thermal and mechanical loads.

The thermal load vector \mathbf{F}_{th} can be written as

$$\mathbf{F}_{th} = \sum_{e=1}^N \int_{v_e} \mathbf{B}_e^T \mathbf{D} \boldsymbol{\varepsilon}_{th}^e dv_e = \sum_{e=1}^N \int_{v_e} \mathbf{B}_e^T \mathbf{D} \boldsymbol{\varphi} \lambda \Delta T dv_e = \sum_{e=1}^N \mathbf{F}_{th}^e, \quad (12)$$

where

$$\mathbf{F}_{th}^e = \int_{v_e} \mathbf{B}_e^T \mathbf{D} \boldsymbol{\varphi} \lambda \Delta T dv_e \quad (13)$$

Here, \mathbf{F}_{th}^e represents the thermal load vector of element e , \mathbf{B}_e is the strain-displacement matrix of element e , N is the total number of elements in the design domain. The change in temperature and the thermal expansion coefficient can be expressed by ΔT and λ , respectively; $\boldsymbol{\varphi}$ is the vector $[1 \ 1 \ 0]^T$.

According to the equilibrium equation,

$$\mathbf{K} \mathbf{U} = \mathbf{F}_m + \mathbf{F}_{th} \quad (14)$$

the structural compliance can be expressed as

$$C = \mathbf{F}_{th}^T \mathbf{U} + \mathbf{F}_m^T \mathbf{U} = (\mathbf{F}_m + \mathbf{F}_{th})^T \mathbf{U} = \mathbf{U}^T \mathbf{K} \mathbf{U} \quad (15)$$

where \mathbf{K} is the global stiffness matrix.

The objective function in Eq. (7) (**structural elastic strain energy**) under a combination of thermal and mechanical loads can be discretized into the finite element format as follows:

$$\begin{aligned} \Phi &= \sum_{i=1}^n \int_{\Omega^i \setminus (\cup_{1 \leq j < i} (\Omega^i \cap \Omega^j))} (\boldsymbol{\varepsilon} - \boldsymbol{\varepsilon}_{th})^T \mathbf{D}^i (\boldsymbol{\varepsilon} - \boldsymbol{\varepsilon}_{th}) dV \\ &= \sum_{i=1}^n \int_{\Omega^i \setminus (\cup_{1 \leq j < i} (\Omega^i \cap \Omega^j))} \boldsymbol{\varepsilon}^T \mathbf{D}^i \boldsymbol{\varepsilon} dV \\ &\quad + \sum_{i=1}^n \int_{\Omega^i \setminus (\cup_{1 \leq j < i} (\Omega^i \cap \Omega^j))} \boldsymbol{\varepsilon}_{th}^T \mathbf{D}^i \boldsymbol{\varepsilon}_{th} dV \\ &\quad - 2 \sum_{i=1}^n \int_{\Omega^i \setminus (\cup_{1 \leq j < i} (\Omega^i \cap \Omega^j))} \boldsymbol{\varepsilon}^T \mathbf{D}^i \boldsymbol{\varepsilon}_{th} dV \end{aligned} \quad (16)$$

It is noteworthy that the elastic strain energy Φ can be categorized into three parts: the first term $\sum_{i=1}^n \int_{\Omega^i \setminus (\cup_{1 \leq j < i} (\Omega^i \cap \Omega^j))} \boldsymbol{\varepsilon}^T \mathbf{D}^i \boldsymbol{\varepsilon} dV$ denotes the work generated by the mechanical and thermal loads on the structural displacement; the second term $\sum_{i=1}^n \int_{\Omega^i \setminus (\cup_{1 \leq j < i} (\Omega^i \cap \Omega^j))} \boldsymbol{\varepsilon}_{th}^T \mathbf{D}^i \boldsymbol{\varepsilon}_{th} dV$ denotes the energy generated by the initial thermal strain and the third term $\sum_{i=1}^n \int_{\Omega^i \setminus (\cup_{1 \leq j < i} (\Omega^i \cap \Omega^j))} \boldsymbol{\varepsilon}^T \mathbf{D}^i \boldsymbol{\varepsilon}_{th} dV$ denotes the work generated by the thermal load on structural displacement. From the

formulations above, the relationship between structural compliance C and elastic strain energy Φ can be expressed as follows:

$$\Phi = C - 2 \sum_{i=1}^n \int_{\Omega^i \setminus (\cup_{1 \leq j < i} (\Omega^i \cap \Omega^j))} \boldsymbol{\varepsilon}^T \mathbf{D}^i \boldsymbol{\varepsilon}_{\text{th}} dV + \sum_{i=1}^n \int_{\Omega^i \setminus (\cup_{1 \leq j < i} (\Omega^i \cap \Omega^j))} \boldsymbol{\varepsilon}_{\text{th}}^T \mathbf{D}^i \boldsymbol{\varepsilon}_{\text{th}} dV \quad (17)$$

The Eq. (17) can be also written as

$$\Phi = C - 2\mathbf{U}^T \mathbf{F}_{\text{th}} + C_{\text{th}} \quad (18)$$

where

$$C_{\text{th}} = \sum_{i=1}^n \int_{\Omega^i \setminus (\cup_{1 \leq j < i} (\Omega^i \cap \Omega^j))} \boldsymbol{\varepsilon}_{\text{th}}^T \mathbf{D}^i \boldsymbol{\varepsilon}_{\text{th}} dV$$

For the structure without thermal load ($\Delta T = 0$), the structural elastic strain energy Φ is equivalent to the structural compliance, however, when the thermal load exists ($\Delta T \neq 0$), the two objective functions are different.

4.2 Sensitivity Analysis

The sensitivity analysis for minimizing the structural compliance and elastic strain energy for the thermoelastic structural topology optimization under the available volume constraint formulated in Eqs. (6) and (7) is presented in this section.

(1) Using **minimum structural compliance** as an objective function, the sensitivity with respect to the design variables a_{ij} (ij represent the j -th design variable of i -th component) can be written as

$$\frac{\partial C}{\partial a_{ij}} = \frac{\partial \mathbf{U}^T}{\partial a_{ij}} \mathbf{K} \mathbf{U} + \mathbf{U}^T \frac{\partial \mathbf{K}}{\partial a_{ij}} \mathbf{U} + \mathbf{U}^T \mathbf{K} \frac{\partial \mathbf{U}}{\partial a_{ij}} \quad (19)$$

Meanwhile, according to

$$\frac{\partial \mathbf{K}}{\partial a_{ij}} \mathbf{U} + \mathbf{K} \frac{\partial \mathbf{U}}{\partial a_{ij}} = \frac{\partial \mathbf{F}_m}{\partial a_{ij}} + \frac{\partial \mathbf{F}_{\text{th}}}{\partial a_{ij}} \quad (20)$$

Substituting Eq. (20) into Eq. (19) results in

$$\frac{\partial C}{\partial a_{ij}} = 2\mathbf{U}^T \left(\frac{\partial \mathbf{F}_m}{\partial a_{ij}} + \frac{\partial \mathbf{F}_{\text{th}}}{\partial a_{ij}} \right) - \mathbf{U}^T \frac{\partial \mathbf{K}}{\partial a_{ij}} \mathbf{U} \quad (21)$$

Because \mathbf{F}_m is a design-independent force, the equation above can be expressed as

$$\frac{\partial C}{\partial a_{ij}} = 2\mathbf{U}^T \frac{\partial \mathbf{F}_{\text{th}}}{\partial a_{ij}} - \mathbf{U}^T \frac{\partial \mathbf{K}}{\partial a_{ij}} \mathbf{U} \quad (22)$$

Furthermore, $\partial \mathbf{F}_{\text{th}}/\partial a_{ij}$ and $\partial \mathbf{K}/\partial a_{ij}$ can be written as

$$\frac{\partial \mathbf{F}_{\text{th}}}{\partial a_{ij}} = \frac{\partial}{\partial a_{ij}} \sum_{e=1}^N \mathbf{F}_{\text{th}}^e = \frac{\partial}{\partial a_{ij}} \sum_{e=1}^N \int_{v_e} \mathbf{B}_e^T \mathbf{D} \boldsymbol{\varphi} \lambda \Delta T dv_e = \frac{E}{4} \left(\sum_{e=1}^N \sum_{\zeta=1}^4 q(H(\phi_e^\zeta))^{q-1} \frac{\partial H(\phi_e^\zeta)}{\partial a_{ij}} \right) \mathbf{F}_{\text{th}}^{e0} \quad (23)$$

$$\frac{\partial \mathbf{K}}{\partial a_{ij}} = \frac{\partial}{\partial a_{ij}} \sum_{e=1}^N \int_{v_e} \mathbf{B}_e^T \mathbf{D} \mathbf{B}_e dv_e = \frac{E}{4} \left(\sum_{e=1}^N \sum_{\zeta=1}^4 q(H(\phi_e^\zeta))^{q-1} \frac{\partial H(\phi_e^\zeta)}{\partial a_{ij}} \right) \mathbf{k}_e^0 \quad (24)$$

where $\mathbf{F}_{\text{th}}^{e0}$ and \mathbf{k}_e^0 is the element thermal load vector and element stiffness matrix corresponding to $H(\phi_e^\zeta) = 1$, $\zeta = 1, \dots, 4$, and $E = 1$. It is noteworthy that the two methods can be used to obtain the value of $\partial H(\phi_e^\zeta)/\partial a_{ij}$, the differential method and the analytical method. The selection of the differential step in the differential method affects the final optimized configuration obviously, however, the appropriate differential step must be performed to obtain better results, which increases the computational cost. Therefore, the analytical method is used in this study, and the specific formulation is as follows:

$$\frac{\partial H(\phi_{\max})}{\partial a_{ij}} = \min(\delta(\phi_i), \delta(\phi_{\max})) \cdot \frac{\partial \phi_i}{\partial a_{ij}} \quad (25)$$

where $\delta = \delta(x)$ denotes the dirac delta function, and i is the number of the components, $i = 1, \dots, n$, $\phi_{\max} = \max(\phi_1, \dots, \phi_n)$.

(2) In case that the **minimum elastic strain energy** as the objective function, according to Eq. (18), then the sensitivity with respect to the design variable a_{ij} can be written as

$$\frac{\partial \Phi}{\partial a_{ij}} = \frac{\partial C}{\partial a_{ij}} - 2 \frac{\partial \mathbf{U}^T}{\partial a_{ij}} \mathbf{F}_{\text{th}} - 2 \mathbf{U}^T \frac{\partial \mathbf{F}_{\text{th}}}{\partial a_{ij}} + \frac{\partial C_{\text{th}}}{\partial a_{ij}} \quad (26)$$

where

$$\frac{\partial C_{\text{th}}}{\partial a_{ij}} = \frac{1}{4} \left(\sum_{\zeta=1}^4 q(H(\phi_e^\zeta))^{q-1} \frac{\partial H(\phi_e^\zeta)}{\partial a_{ij}} \right) C_{\text{th}}^0 \quad (27)$$

where, C_{th}^0 denotes the energy generated by the initial thermal strain corresponding to $E = 1$. $\partial \mathbf{U}^T/\partial a_{ij}$ can be obtained from Eq. (20), $\partial C/\partial a_{ij}$ and $\partial \mathbf{F}_{\text{th}}/\partial a_{ij}$ can be obtained from Eqs. (22) and (23), respectively.

5 Numerical Examples and Discussions

In this section, a benchmark example is used to verify the effectiveness of the MMC-based framework in topology optimization of thermoelastic structures, and the effects of different objective functions on the structural topology configurations are compared. Furthermore, the physical meaning of the different objective functions is discussed. The design variable updating strategy adopted in this study is the method of moving asymptotes (MMA) [32]. In this section, it is assumed that the structure is in the state of plane stress, the unit of thickness is 1, and the finite element is in the form of a bilinear four-node rectangular element. In the example, the geometrical, material, and load parameters are in dimensionless forms.

5.1 A Two-End Clamped Beam with Only a Mechanical Load

The purpose of this example is to verify the advantages of the proposed topology optimization framework. A two-end clamped beam with $H \times L = 1 \times 2$ design domain is investigated, which is discretized using a 80×160 mesh for finite element analysis; and a downward unit point mechanical load is applied at the bottom center of the domain, as shown in Fig. 4a. The Young's modulus and the Poisson's ratio of the material were $E = 1$, and $\mu = 0.3$, respectively. Sixteen components are used for the initial building blocks for the MMC-based topology optimization framework, as illustrated in Fig. 4b, and the total number of design variables is $16 \times 5 = 80$, in which 5 design variables in one component. This example only considers the minimum structural compliance as the objective function, with a 10% available volume constraint.

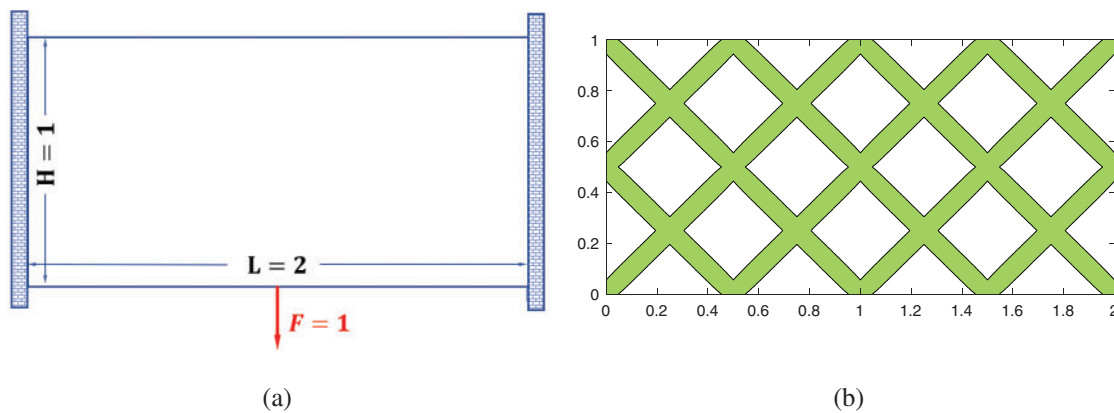


Figure 4: First example: (a) a two-end clamped beam design domain only with a mechanical load, (b) initial building blocks of MMC-based framework

For the design domain, as shown in Fig. 4a, the corresponding optimization problem with only a mechanical load can be solved using an analytical method, which was described in detail by Yan et al. [13]. According to the [13], the corresponding optimal inclined angle of the final two-bar structural topology is $\theta^{\text{opt}} = \pi/4$ for the structure described in Fig. 5b, because the length of the design domain is twice of its width. In this section, the density-based (SIMP) and MMC-based methods are both used to calculate the optimal topology of this example numerically, which is then compared with the analytical solution. The optimized configurations under this case obtained by density-based and MMC-based methods are shown in Fig. 5. The numerical results show that the objective value from the MMC-based method agreed well with the density-based method and is slightly better than that of the density-based method. The inclined angle of components of the optimized configuration to the horizontal direction is 45° as shown in Fig. 5a, and agreed well with the analytical result in [13], which validates the optimization model and algorithm established in this study. Fig. 5b shows the optimized topology obtained by the density-based method, in which the geometric profile is relatively unclear in some extends because of gray elements in the final optimized topology. For thermal problems, the presence of gray elements in the optimized structure will cause the following problems: firstly, in the heat transfer problem, it will be hard to determine whether the edge of the heat sink is in contact with the other structure, which will result in the inability to accurately evaluate the performance of the heat sink; secondly, in the thermal convection problem, it is difficult to accurately parameterize the convection through the gray elements, and it is necessary to introduce coefficients for correction to perform thermal

convection calculation [33]; lastly, because the thermal load is design-dependent load, when dealing with the coupled thermoelastic problem, the gray element will cause the inability to accurately calculate the magnitude of the thermal load, which affects the coupled thermal analysis of the structure. The optimized topology configuration by the MMC-based method shows a clear geometric profile, as shown in Fig. 5a, which avoiding the “gray” elements difficulties. Therefore, the MMC-based method is used to study the thermoelastic topology optimization problem to compare the optimization effect from different objective functions in the following sections.

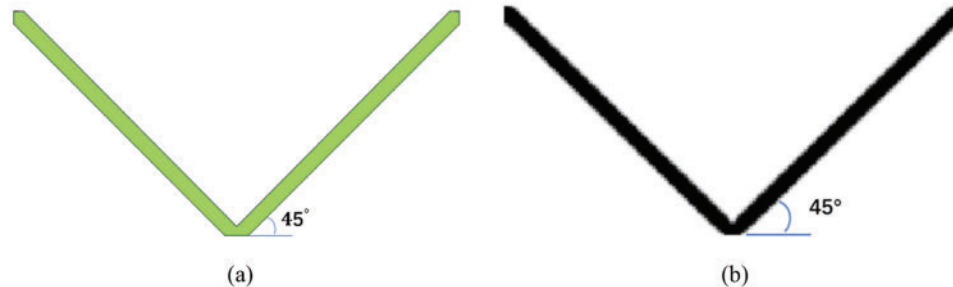


Figure 5: The optimized configurations obtained by different methods. (a) The optimized configuration from MMC-based framework with the compliance $C = 22.177$. (b) The optimized configuration from density-based method with the compliance $C = 23.932$

5.2 A Two-End Clamped Beam with Thermo-Mechanical Load

The same two-end clamped beam, as shown in Fig. 4a, with both thermal and mechanical loads, is studied in this example. The structure is subjected to a uniform temperature $\Delta T = 100$ higher than the reference temperature, whereas the Young’s modulus and Poisson’s ratio of the material are the same as those in the example in Section 5.1, and the thermal expansion coefficient is $\lambda = 1 \times 10^{-2}$, the material parameters remain constant with temperature changes. The minimum structural compliance is used as the optimization objective. The effects of different volume fractions and different temperatures on the optimized structural topology are discussed as shown in Fig. 6.

Fig. 6a shows the effects of different volume fractions on the optimized topological configurations. As we can observe from Fig. 6a, a two-bar V-shaped configuration of the optimized configurations does not change as the volume fraction increases but the objective function value of the structure decreased gradually as the specified volume fraction increased. However, when the base material of the structure continued to increase, the degree of reduction of the structural compliance became stable gradually, indicating that increasing the material can no longer reduce the compliance of the structure significantly when the volume fractions are greater than 0.4 in this example.

To further investigate the effect of temperature changes on the optimized structural layout, the two-end clamped beam structure with different temperature changes is optimized under the same volume fraction. As shown in Fig. 6b, with the increase of the temperature change, the compliance of the structure is continuously increased, and the optimized topology of structures differs with the increasing temperature. In addition, a sudden transformation of configuration occurs within the temperature changes range of 175~225, the structural configuration changes from a two-bar V-shaped structure to a three-bar “claw-like” structure. When the temperature is

relatively low, the layout of the optimized structure is a two-bar V-shaped because the mechanical load is the dominant load at this time. As the temperature changes increased, the effect of the thermal load becomes more and more prominent, and the optimized configurations changed from a two-bar V-shaped to a three-bar “claw-like” structure. This configuration indicates that the deformation caused by the thermal load and mechanical load offset each other, thereby reducing the work performed by the combination of thermal and mechanical loads and reducing the structural compliance. Furthermore, Fig. 6b illustrates that temperature changes significantly affect the optimized configuration of the thermoelastic structure.

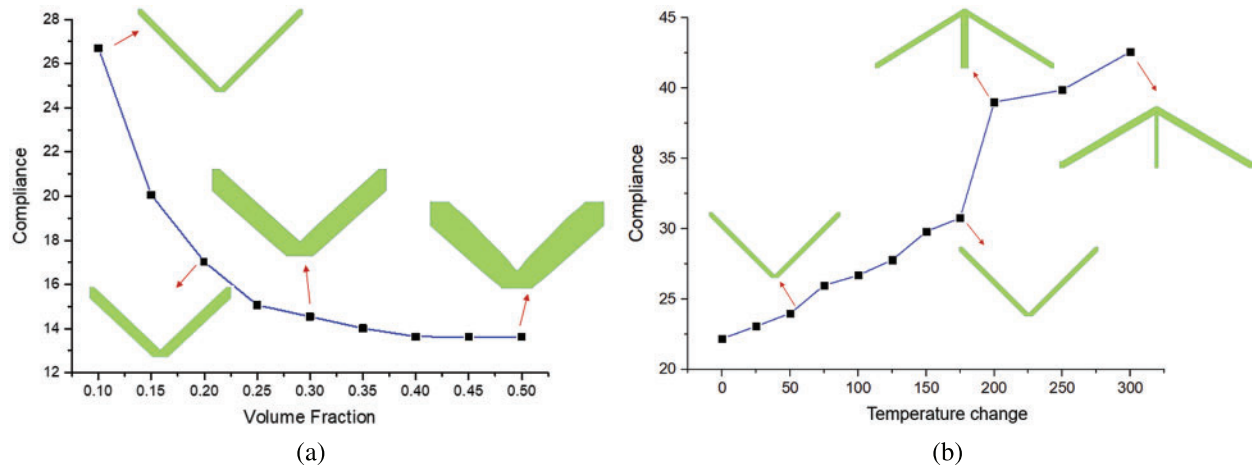


Figure 6: The optimized topological configurations with the objective function of compliance considering thermal and mechanical loads. (a) Effect of different volume fractions on the optimized topological configuration, (b) Effect of temperature changes on the optimized topological configuration

As can be seen from Fig. 6b, the optimized results are both three-bar “claw-like” structures when the temperature changes are 200 and 300, respectively. However, some slight differences exist between the two structures. When the temperature change is 200, the middle rod of the optimized topology structure is thicker and the two inclined bars are thinner. However, when the temperature change is 300, the middle bar of the optimized topology becomes thinner, and the two inclined bars are thicker. This is because the thermal load effect is more obvious in the case of $\Delta T = 300$, the mechanical load is not dominant at this time, and the two inclined thicker bars help to resist the thermal loading effect.

However, the structural compliance represents the total work generated by a specified load (mechanical or thermal load). When a structure is subjected to a mechanical load, the compliance of the structure represents the measurement of the volume and shape changes caused by the mechanical loads. However, when the structure is subjected to a combination of thermal and mechanical loads, the physical meaning of the compliance of the structure is questionable. The structural deformation cannot guarantee to be minimized in this case. Furthermore, from Fig. 7c and Tab. 1, we can observe a relatively high-stress level in the optimized structure, in which the optimized three-bar “claw-like” configuration applies more strict constraint on the structural deformation.

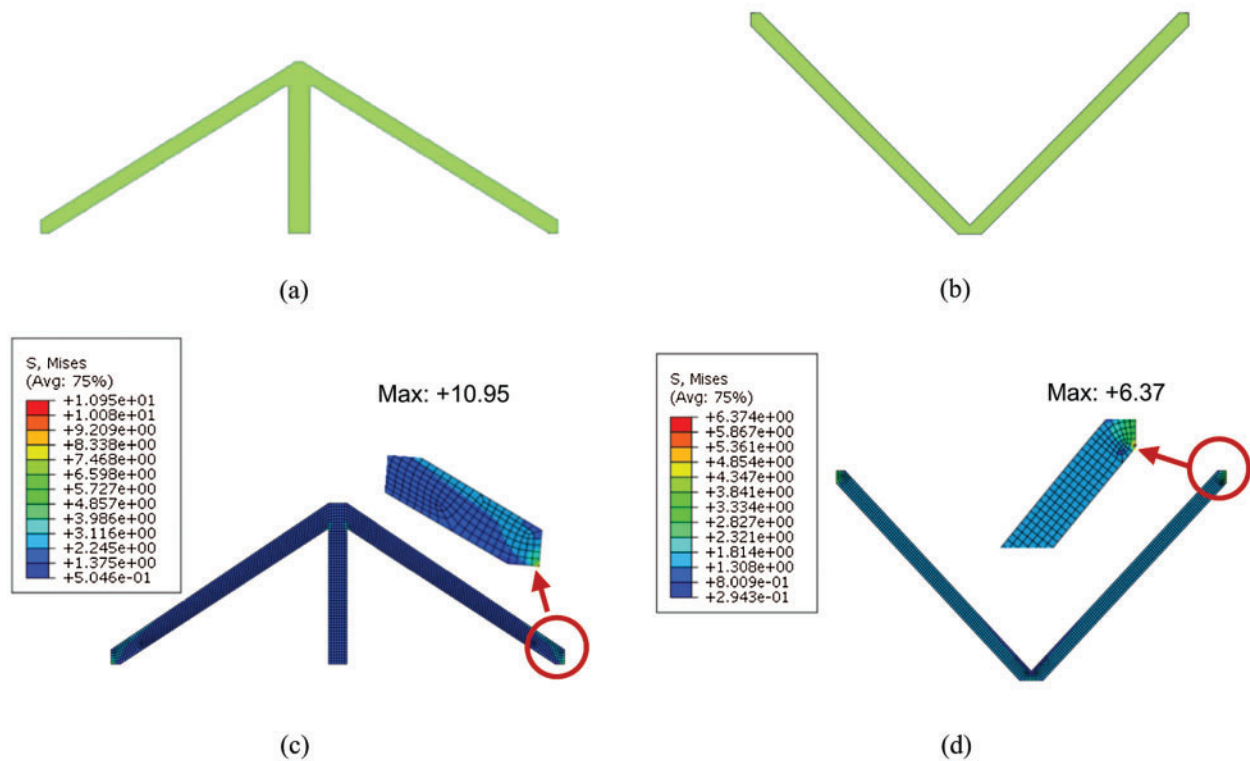


Figure 7: Optimized topological configurations and corresponding Mises stress nephograms obtained by two types of objective functions when $\Delta T = 200$. (a) The optimized topological configuration obtained by minimum compliance optimization. (b) The optimized topological configuration obtained by minimum strain energy optimization. (c) The Mises stress nephograms of the optimized topological configuration with minimum compliance optimization, maximum Mises stress is 10.95. (d) The Mises stress nephograms of the optimized topological configuration with minimum strain energy optimization, maximum mises stress is 6.37

Table 1: Maximum mises stress of optimized results obtained by different objective function

Case	Maximum mises stress obtained by compliance optimization	Maximum mises stress obtained by strain energy optimization
$\Delta T = 50$	1.613	1.141
$\Delta T = 100$	2.565	1.988
$\Delta T = 150$	3.550	2.996
$\Delta T = 200$	4.546	4.114
$\Delta T = 250$	5.548	5.235
$\Delta T = 300$	6.553	6.358

To considering the effects of structural stress, the minimum elastic strain energy is chosen as another type of objective function to obtain the optimized topology of the thermoelastic structure. To compare the different structural configurations obtained by the two types of objective functions at the same temperature changes, the optimized configurations at $\Delta T = 200$ are given in

Figs. 7a and 7b. The Mises stress of the two configurations are calculated by ABAQUS [34] and presented in Figs. 7c and 7d, respectively. The maximum Mises stress of the optimized configuration with the minimum compliance as the objective function is 10.95 presented in Fig. 7c, whereas that with the minimum strain energy as the objective function is 6.37 in Fig. 7d. This is because the two-bar V-shaped configuration obtained from the minimum elastic strain energy formulation can relatively easily relax the constraints on structural deformation and reduce the thermal stress of the structure, which can be seen from the stress nephogram.

The finite element analysis in Figs. 7c and 7d, an 8-node biquadratic element is adopted to ensure the convergence of the Mises stress values of different mesh densities at the same temperature. Fig. 8 shows the effect of temperature changes on the optimized configurations obtained by minimum strain energy optimization. Then it can be seen from Fig. 8 that the optimized configuration based on minimum strain energy always presented a two-bar V-shaped configuration for all the temperature change cases, which is obviously difference with that observed in compliance optimization (changing from a two-bar V-shaped configuration to a three-bar “claw-like” configuration).

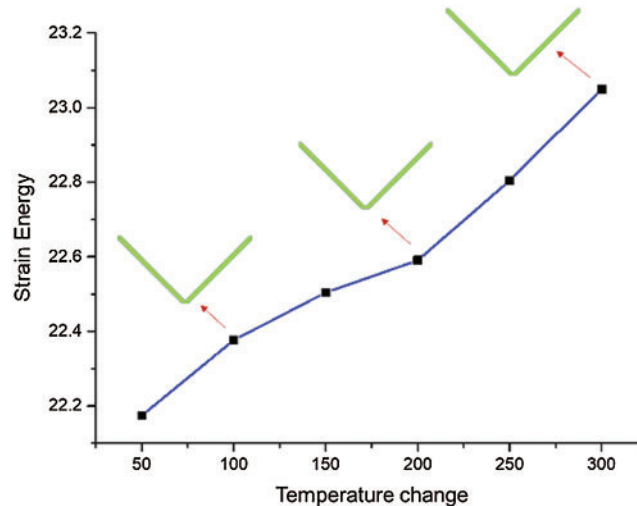


Figure 8: The Effect of temperature on structural strain energy

It is especially pointed that for a better comparison, the mechanical load is set as $F = 0.1$ (compared with Fig. 4a), Tab. 1 shows the maximum Mises stress values at different temperature changes with minimum compliance and minimum strain energy as the objective functions. The results show that setting the strain energy minimization as the objective function can reduce the stress and provide a better strength design compared with that from compliance minimization for the same thermoelastic structure.

Tab. 2 shows the comparison of the maximum displacement values of the two topological configurations obtained based on the two different objective functions at different temperature changes. As show in Tab. 2, when the temperature changes are relatively low, such as $\Delta T = 50$ or $\Delta T = 100$, the maximum deformations of the optimized configurations obtained from the minimum compliance design are smaller than that obtained from minimum strain energy design. However, when the temperature change are relatively large, such as $\Delta T > 150$, the maximum

deformations of the optimized configurations obtained from the minimum strain energy design are smaller than that obtained from the minimum compliance design. Therefore, different from the compliance optimization in the topology optimization only with mechanical loads which gives the minimum deformation design, the compliance design of the thermoelastic structure does not always give the minimum deformation design.

Table 2: Maximum displacement of optimized results obtain by different objective function

Case	Maximum displacement obtained by compliance optimization	Maximum displacement obtained by strain energy optimization
$\Delta T = 50$	5.40	8.69
$\Delta T = 100$	14.01	15.41
$\Delta T = 150$	22.63	22.14
$\Delta T = 200$	31.25	28.86
$\Delta T = 250$	39.87	35.58
$\Delta T = 300$	48.50	42.30

Combined with [Tabs. 1](#) and [2](#), it can be observed that when the objective function of the minimum strain energy of the structure is used, the maximum Mises stress of the optimized structure is always lower than that from compliance design, while the maximum displacement values of the optimized structure designed with the minimum compliance and that with the minimum strain energy have no consistent magnitude relationship. Therefore, for the topological optimization design of a thermoelastic structure, the physical significance of taking the minimum compliance as the objective function is not clear, and the performance of the optimized configurations obtained is not well predicted.

6 Conclusions

In the present study, to overcome the challenges of traditional topological optimization methods for addressing thermoelastic topology optimization, the MMC-based topology optimization framework is applied. Topology optimization design is performed using the minimum compliance and minimum strain energy as the objective functions, with a specified available volume constraint. Subsequently, the response of the optimized structural topology under the combination of thermal and mechanical loads is investigated. The topological optimization formulation and the derivation of analytical sensitivity are presented, and the physical meanings of different objective functions are discussed separately. When using the minimum compliance as the objective function for topology optimization design, the thermal load exerted a certain effect on the topological configuration of the structure. The topological configuration of the structure changed from a two-bar V-shaped structure to a three-bar “claw-like” structure. Such a configuration transformation is beneficial to reduce the compliance of the structure but increases the level of stress inside the structure. However, when using the minimum strain energy as the objective function for topology optimization design, there is no topology changing observed as the thermal load increased. This occurred because the minimum strain energy of the structure indicates the stress level of the structure, and the two-bar V-shaped structure obtained from the minimum elastic strain energy formulation is beneficial for relaxing the structural deformation constraints. In addition, the results indicate that by utilizing the minimum strain energy as the objective function, compared with

compliance minimization, the structural configurations obtained are more superior in terms of structural strength.

Funding Statement: Financial supports for this research were provided by the National Natural Science Foundation of China (Nos. 11672057, 12002278, U1906233), the National Key R&D Program of China (2017YFC0307201), the Key R&D Program of Shandong Province (2019JZZY010801), the Fundamental Research Funds for the Central Universities (NWPU-G2020KY05308). These supports are gratefully acknowledged.

Conflicts of Interest: The authors declare that they have no conflicts of interest to report regarding the present study

References

1. Guo, X., Cheng, G. D. (2010). Recent development in structural design and optimization. *Acta Mechanica Sinicalixue Xuebao*, 26(6), 807–823. DOI 10.1007/s10409-010-0395-7.
2. Rozvany, G. I. N. (2009). A critical review of established methods of structural topology optimization. *Springer*, 37(3), 217–237. DOI 10.1007/s00158-007-0217-0.
3. Sigmund, O., Maute, K. (2013). Topology optimization approaches: A comparative review. *Structural and Multidisciplinary Optimization*, 48(6), 1031–1055. DOI 10.1007/s00158-013-0978-6.
4. Takezawa, A., Yoon, G. H., Jeong, S. H., Kobashi, M., Kitamura, M. (2014). Structural topology optimization with strength and heat conduction constraints. *Computer Methods in Applied Mechanics and Engineering*, 276, 341–361. DOI 10.1016/j.cma.2014.04.003.
5. Ni, X. Q., Cheng, G. D. (2015). Optimal design of thin solid elastic plates under thermal load. *Applied Mathematics and Mechanics*, 36(3), 233–241. DOI 10.3879/j.issn.1000-0887.2015.03.001.
6. Rodrigues, H., Fernandes, P. (1995). A material based model for topology optimization of thermoelastic structures. *International Journal for Numerical Methods in Engineering*, 38(12), 1951–1965. DOI 10.1002/(ISSN)1097-0207.
7. Sigmund, O., Torquato, S. (1997). Design of materials with extreme thermal expansion using a three-phase topology optimization method. *Journal of the Mechanics and Physics of Solids*, 45(6), 1037–1067. DOI 10.1016/S0022-5096(96)00114-7.
8. Li, Q., Steven, G. P., Xie, Y. X. (1999) Displacement minimization of thermoelastic structures by evolutionary thickness design. *Computer Methods in Applied Mechanics and Engineering*, 179(3–4), 361–378. DOI 10.1016/S0045-7825(99)00047-X.
9. Li, Q., Steven, G. P., Xie, Y. M. (2001). Thermoelastic topology optimization for problems with varying temperature fields. *Journal of Thermal Stresses*, 24(4), 347–366. DOI 10.1080/01495730151078153.
10. Cho, S., Choi, J. Y. (2005). Efficient topology optimization of thermo-elasticity problems using coupled field adjoint sensitivity analysis method. *Finite Elements in Analysis and Design*, 41(15), 1481–1495. DOI 10.1016/j.finel.2005.05.003.
11. Chung, H., Amir, O., Kim, H. A. (2020). Level-set topology optimization considering nonlinear thermoelasticity. *Computer Methods in Applied Mechanics and Engineering*, 361, 112735. DOI 10.1016/j.cma.2019.112735.
12. Deng, J., Yan, J., Cheng, G. (2013). Multi-objective concurrent topology optimization of thermoelastic structures composed of homogeneous porous material. *Structural and Multidisciplinary Optimization*, 47(4), 583–597. DOI 10.1007/s00158-012-0849-6.
13. Yan, J., Guo, X., Cheng, G. (2016). Multi-scale concurrent material and structural design under mechanical and thermal loads. *Computational Mechanics*, 57(3), 437–446. DOI 10.1007/s00466-015-1255-x.
14. Li, L., Kim, H. A. (2020). Multiscale topology optimization of thermoelastic structures using level set method. *AIAA Scitech 2020 Forum*, vol. 1. American Institute of Aeronautics and Astronautics Inc., AIAA. Orlando, FL, USA. DOI 10.2514/6.2020-0890.

15. Zhu, X., Zhao, C., Wang, X., Zhou, Y., Hu, P. et al. (2019). Temperature-constrained topology optimization of thermo-mechanical coupled problems. *Engineering Optimization*, 51(10), 1687–1709. DOI 10.1080/0305215X.2018.1554065.
16. Wu, C., Fang, J., Li, Q. (2019). Multi-material topology optimization for thermal buckling criteria. *Computer Methods in Applied Mechanics and Engineering*, 346, 1136–1155. DOI 10.1016/j.cma.2018.08.015.
17. Gao, T., Zhang, W. (2010). Topology optimization involving thermo-elastic stress loads. *Structural and Multidisciplinary Optimization*, 42(5), 725–738. DOI 10.1007/s00158-010-0527-5.
18. Li, L., Du, Z., Kim, H. A. (2020). Design of architected materials for thermoelastic macrostructures using level Set method. *JOM*, 72(4), 1734–1744. DOI 10.1007/s11837-020-04046-2.
19. Pedersen, P., Pedersen, N. L. (2010). Strength optimized designs of thermoelastic structures. *Structural and Multidisciplinary Optimization*, 42(5), 681–691. DOI 10.1007/s00158-010-0535-5.
20. Pedersen, P., Pedersen, N. L. (2012). Interpolation/penalization applied for strength design of 3D thermoelastic structures. *Structural and Multidisciplinary Optimization*, 45(6), 773–786. DOI 10.1007/s00158-011-0755-3.
21. Deaton, J. D., Grandhi, R. V. (2013). Stiffening of restrained thermal structures via topology optimization. *Structural and Multidisciplinary Optimization*, 48(4), 731–745. DOI 10.1007/s00158-013-0934-5.
22. Deaton, J. D., Grandhi, R. V. (2016). Stress-based design of thermal structures via topology optimization. *Structural and Multidisciplinary Optimization*, 53(2), 253–270. DOI 10.1007/s00158-015-1331-z.
23. Zhang, W., Yang, J., Xu, Y., Gao, T. (2014). Topology optimization of thermoelastic structures: Mean compliance minimization or elastic strain energy minimization. *Structural and Multidisciplinary Optimization*, 49(3), 417–429. DOI 10.1007/s00158-013-0991-9.
24. Meng, Q., Xu, B., Wang, C., Zhao, L. (2020). Stress constrained thermo-elastic topology optimization based on stabilizing control schemes. *Journal of Thermal Stresses*, 43(8), 1040–1068. DOI 10.1080/01495739.2020.1766391.
25. Bruyneel, M., Duysinx, P. (2005). Note on topology optimization of continuum structures including self-weight. *Structural and Multidisciplinary Optimization*, 29(4), 245–256. DOI 10.1007/s00158-004-0484-y.
26. Xia, Q., Wang, M. Y. (2008). Topology optimization of thermoelastic structures using level set method. *Computational Mechanics*, 42(6), 837–857. DOI 10.1007/s00466-008-0287-x.
27. Guo, X., Zhang, W., Zhong, W. (2014). Doing topology optimization explicitly and geometrically—A new moving morphable components based framework. *Journal of Applied Mechanics, Transactions ASME*, 81(8), 1–12. DOI 10.1115/1.4027609.
28. Zhang, W., Yuan, J., Zhang, J., Guo, X. (2016). A new topology optimization approach based on moving morphable components (MMC) and the ersatz material model. *Structural and Multidisciplinary Optimization*, 53(6), 1243–1260. DOI 10.1007/s00158-015-1372-3.
29. Zhang, W., Li, D., Kang, P., Guo, X., Youn, S. K. (2020). Explicit topology optimization using IGA-based moving morphable void (MMV) approach. *Computer Methods in Applied Mechanics and Engineering*, 360, 112685. DOI 10.1016/j.cma.2019.112685.
30. Zhang, W., Jiang, S., Liu, C., Li, D., Kang, P. et al. (2020). Stress-related topology optimization of shell structures using IGA/TSA-based moving morphable void (MMV) approach. *Computer Methods in Applied Mechanics and Engineering*, 366, 113036. DOI 10.1016/j.cma.2020.113036.
31. Takaloozadeh, M., Yoon, G. H. (2017). Implementation of topological derivative in the moving morphable components approach. *Finite Elements in Analysis and Design*, 134, 16–26. DOI 10.1016/j.finel.2017.05.008.
32. Svanberg, K. (1987). The method of moving asymptotes—A new method for structural optimization. *International Journal for Numerical Methods in Engineering*, 24(2), 359–373. DOI 10.1002/(ISSN)1097-0207.
33. Deaton, J. D., Grandhi, R. V. (2014). A survey of structural and multidisciplinary continuum topology optimization: Post 2000. *Structural and Multidisciplinary Optimization*, 49(1), 1–38. DOI 10.1007/s00158-013-0956-z.
34. ABAQUS (2014). ABAQUS v.6.14-2 Commercial FE Software and Documentation. Dassault Systèmes. Simulia Corporation, Providence, RI, USA.